Analysis of Structural, Electronic and Mechanical Properties of $Cr_xSn_{1-x}O_2$ Compounds from First Principle Approach

Ayedun, F.[1], Bamgbose, M. K.[2], Solola, G. T.[3], Adebambo, P. O.[4], Agbaoye, R. O.[5], Agbogu, A. C.[6], Lawal, T. O.[7], Kolo, M. T.[8]

[1,*]Department of Physics, National Open University of Nigeria, Abuja

[2]Department of Physics, Lagos State University, Ojo, Nigeria

[3]Department of Physics, Augustine University Ilara, Epe, Nigeria

[4]Department of Physics, Federal University of Agriculture, P.M.B.2240 Abeokuta, Nigeria

[5]Applied Science Department, Federal College of Dental Technology and Therapy Enugu, Enugu State, Nigeria

[6]Department of Physics, University of Nigeria, Nsukka, Enugu, Nigeria

[7]Department of Physics, University of Ilorin, Ilorin, Kwara State, Nigeria

[8]Department of Physics, Federal University of Technology, Minna, Niger State, Nigeria

*Corresponding author: fayedun@noun.edu.ng

ABSTRACT: In this work, the elastic constants of the second-order rutile $Cr_xSn_{1-x}O_2$ compounds were investigated using the first- principle methods. From here, we obtained the effects of Cr atoms on SnO_2 which enhanced increase in an isotropic bulk modulus, shear modulus, sound velocities as well as Debye temperature θ. The direct energy band gaps of $Cr_xSn_{1-x}O_2$ compounds decreased with the addition of Cr atom from x = 0 to 1. However, the energy band gap computation showed decrease in an indirect gap from x = 0.25 to 0.75 and increase at x = 1 as the molar fraction of chromium atom added varied. The calculated Poisson's ratio revealed mechanical stability and ductility of $Cr_xSn_{1-x}O_2$ compounds. This study analysed the computed pressure with Birch-Murnagan expression at x = 0(413.0GPa), x = 0.25(577.1GPa), x = 0.50(663.2GPa), x = 0.75 (907.7GPa) and x = 1.00(660.1GPa).

KEYWORDS: First principle, Transition Metallic-oxide, Density functional theory, Elastic Properties, Electronic properties.

1. INTRODUCTION

The tetragonal rutile structured stannic oxide with the space group $P4_2/mnm$ is the primary ore from unformed tin with a chemical composition of tin oxide (SnO_2) mainly found in veins of rough igneous rocks. The pure binary SnO_2 is colourless, diamagnetic and amphoteric. SnO_2, an n-type broad bandgap transition metallic oxide, is attracting significant attention due to its relevance as an opacifier (Molera et al., 2004), catalyst(Lee et al.,2020;Bejtka et al., 2019; Mauraya et al., 2020), pigment in the manufacturing of glasses and enamels (Trojan et al.,2016; Topuz et al., 2016), polishing powder (Sikalidis, 2011), conductive coatings (Yao et al.,2019; Yang et al., 2006), refractories (Jedynak et al., 2011), solar cells (Liu et al., 2019), gas sensing(Rieu et al., 2015), electrochemical (Biswal et al., 2020; Kuriganova et al., 2016) and medicine(Gorai, 2018 and Kuriganova et al., 2016) to mention a few.

The peculiar applications of bulk SnO_2 enhanced its in-depth studies both experimentally (Schierbaum et al., 1991; Das et al., 2016; Jim et al.,2014) and theoretically (Akgul et al., 2013; Liu et al., 2011; Oshima and Yoshino 2012;

Fakhim et al., 2014; Robertson, 1979; Godinho et al., 2009; Li et al., 2009;Ozer and Cabuk 2019) using various approaches (Mauraya et al., 2020; Diliegros-Godines et al; 2015; Sharma et al.,2010; Gao et al., 2014). Akgul et al., (2013) in an experimental survey, determined structural, optical and electronic properties of the polycrystalline thin film of fluorine doped tin oxide (FTO) at 400^{o}C using spray pyrolysis approach. Gao et al., (2014) studied the betterment of mechanical properties of FTO thin films and discovered an increase in its hardness and Young modulus from 9.01GPa to 15.08 GPa and 125.24GPa to 206.93 GPa, respectively. Ozer and Cabuk (2019) derived pressure- dependence empirical equations of the elastic constant and determined structural and elastic properties of rutile cassiterite at ambient and under pressures. Godinho et al., (2009) explored density functional theory (DFT) to compute the formation energies and electronic properties of possible isolated defects and their clustered pairs. Other researchers such as: Haeberie et al., (2016); Henkel et al., (2019); Sabergharresou et al., (2019); Leng et al., (2012) and Borges et al. (2011) also embarked on various studies.

The mechanical property displays the durability and range of usage of any material subject to applied force. It is influenced by features like grain size, heat treatment, atmospheric exposure, temperature, modulus of elasticity, tensile strength elongation, hardness, fatigue limit, conductivity, corrosion resistance, density, fracture toughness, plasticity, melting point and coefficient of friction (Liu etal., 2011). Materials elasticity depends on these three moduli: Young's modulus, bulk modulus and shear modulus. The extension of the elastic limit of materials due to stress results in fracture or plastic behaviours.

Notwithstanding the volume of existing works on SnO_2, there is a need to examine the effects of dopant; chromium on SnO_2, its structural, electronic and elastic properties at various concentrations to enhance elongation of new materials and their usefulness under an applied force.

2. COMPUTATIONAL DETAILS

The structural, mechanical and electronic properties of $Cr_x Sn_{1-x} O_2$ compounds were determined in this study using Perdew-Burke Ernzhof- Projected Augmented Wave (PBE-PAW) from quantum espresso package and its cost- efficient, inside Generalized Gradient Approximation (GGA) about density functional theory. The Monkhorst Pack (Monkhorst and Pack, 1976).

K-mesh is sampled at 10x10x5 at x = 0.00, 0.25, 0.75 and 1.00 also, 8x8x4 at x = 0.50. The kinetic energy cut off is set at 80.0eV at x = 0 and 90.0eV at x = 0.25 to 1.00. The consistent self-convergence of total energy is set at 0.01 mRy. The outer valence electrons for the pseudo-atom quantum simulations are: Sn $5S^2 5P^2$, O $2S^2 2P^4$ and Cr $3d^5 4s^1$.

3. METHODOLOGY

Vegard's principle examined the rules of energy mixture of solid solution between two phases A and B at constant temperature and uniform crystal structure. The rule is not restricted to only pure binary solid solution A and B, it is

also applicable to ternary transition metallic oxide, $Cr_x\,Sn_{1-x}O_2$. The Energy gap (E_g) as demonstrated by Vergard's principle is:

The energy band gaps at x = 0 to 1 for each substitution of Cr atom into SnO_2 were computed using Vegard's law (Vegard, 1921):

$$E_g\,(A_x\,B_{1-x}\,C) = x\,E_{AC} + (1-x)\,E_{BC} \qquad (1)$$

while, E_{AC} and E_{BC} are the equilibrium band energies of CrO_2, SnO_2 and $E_g\,(A_x\,B_{1-x}\,C)$ is the energy gap for the ternary compound. Because of lack of compliance to Vergard's principle in semiconductors both theoretical (Ayedun et al., 2017; Rashkeev and Lambrecht 2001) and experimental works (Ayedun et al., 2017), this principle can now be written as:

$$E_g(A_xB_{1-x}C) = xE_{AC} + (1-x)\,E_{BC} - x(1-x)b_E, \qquad (2)$$

where b_E stands for bowing constant.

3.1 Elastic Constants

Elastic constants such as Young modulus, Bulk modulus, shear modulus and Poisson's ratio describe the elastic behavior of materials. Flexible materials with high modulus are rigid, and the ones with low modulus easily yield to deformation. Elasticity is pronounced in solids than liquids. In solids, the atomic lattice changes size and shape when forces are applied. Hook's law of elasticity is obeyed when material regains its original shape and size. Hook's law can be expressed as:

$$\sigma = \quad C\varepsilon,$$

where σ is the Cauchy stress tensor, ε is the minute strain tensor and C is the fourth-order stiffness tensor which can be reduced to an elasticity matrix, given thus:

$$C_{ijkl} = \begin{bmatrix} C_{11} & C_{12} & C_{13} & C_{14} & C_{15} & C_{16} \\ C_{12} & C_{22} & C_{23} & C_{24} & C_{25} & C_{26} \\ C_{13} & C_{23} & C_{33} & C_{34} & C_{35} & C_{36} \\ C_{14} & C_{24} & C_{34} & C_{44} & C_{45} & C_{46} \\ C_{15} & C_{25} & C_{35} & C_{45} & C_{55} & C_{56} \\ C_{16} & C_{26} & C_{36} & C_{46} & C_{56} & C_{66} \end{bmatrix} \qquad (4)$$

The Cauchy stress quantifies the stress used for small strains while the infinitesimal shear tensor measures applied strain. Altogether, there are twenty-one independent elastic constants. The number of independent tensor elastic constants is a function of the symmetry of the crystal. SnO_2 is a tetragonal structure, and only six independent

tensors elastic constant is made use of, namely: C_{11}, C_{12}, C_{13}, C_{33}, C_{44} and C_{66} according to Liu (2011). The absolute requirements for the elastic stability of tetragonal crystals under isotropic pressures are:

$$\begin{aligned} &C_{11} > 0,\ C_{33} > 0, C_{44} > 0, C_{66} > 0 \\ &(C_{11} - C_{12}) > 0, (C_{11} + C_{33} + 2C_{13}) > 0 \\ &(2C_{11} + 2C_{12} + C_{33} + 4C_{13}) \end{aligned} \quad (5)$$

Voight-Reuss-Hill approximation is a device useful in calculating isotropic polycrystalline elastic moduli and it is applied in this study to evaluate Bulk, Young's and Shear modui, and Poisson's ratio as revealed in Tables 3 and 4. After that, we determined bulk velocity (V_B), elastic waves velocity comprising compressional(V_P) and shear wave (V_G) velocities at various concentrations x = 0 to 1 from Navier's equation (Liu et al., 2011):

$$V_p = \sqrt{(B_s + (4/3)G)/\rho} \qquad V_s = \sqrt{\frac{G}{\rho}} \quad (6)$$

Herein, G denotes shear modulus, B_s depicts adiabatic bulk modulus and ρ stands for density.

4. RESULTS AND DISCUSSION

4.1 Structural Properties

The earliest calculation performed in this study was on the investigation of crystals' structure. The lattice parameters a and $\frac{c}{a}$ were varied simultaneously in ± 5 spaces within the span of 0.01. The computed total energies (E) at different volumes (V) were perfectly fitted into the second-order Birch-Murnagan equation of state. The exchange Murnagan (Birch, 1947 and Murnagan, 1944) equation of state is:

$$\delta E(V) = E - E_o = BV_o\left[\frac{V_n}{B'}\right] + \left(\frac{1}{(1-B')}\right) + \left(\frac{V_n}{B'(B'-1)}\right) \quad (7)$$

It was observed that both computed equilibrium volumes and pressure increase in value with added Cr atoms from x = 0 (490.43Å^3, 413.0 GPa),x = 0.25 (942.99Å^3, 577.1 GPa). At x = 0.50(939.61 Å^3, 663.2 GPa); x = 0.75 (912.07Å^3, 907.7 GPa). The two reduced from x = 0.75 and crystallized into CrO_2 (863.10Å^3, 660.1GPa) at x = 1.

$Cr_x Sn_{1-x} O_2$ compound retained its tetragonal crystal structures for a pure SnO_2 with a six atom supercell at x = 0 and when Cr atom replaced Sn atom from x =0.25 to 1 using a twelve atom supercell with atomic positions Sn: 2a (0, 0, 0), (0.5, 0.5, 0.5) and O: 4f (0.305, 0.305, 0), (0.695, 0.695, 0), (0.195, 0.805, 0.5), (0.805, 0.195, 0.5). The ground state structural parameters of a, c, bulk modulus (B) and its derivative B' are displayed in table 1. The results of the unit cell (a and c) are in harmony with existing results (Letifi et al., 2019 and Rahman et al., 2008). The values of bulk modulus (B) and its derivative B' are slightly higher because of the GGA artefact.

Table 1: Optimized Lattice parameters a, c, bulk modulus (B) and pressure derivative of SnO_2.

Parameter	**Present Study**	**Existing Works**	
		Experimental	**Theoretical**
a (Å)	4.7358	4.743, 4.7202, 4.7471	4.8959, 4.780
c	3.1853	3.2070, 3.200	3.0371, 3.268
B [GPa]	413.0	205, 270	213.69, 244.7
B´[GPa]	9.63	7	6

4.2 Electronic Properties

The computed band structure energies of $Cr_x Sn_{1-x} O_2$ compound are depicted in Figures 1a-e. Both direct and indirect energy gaps from uppermost valence band to minimum conduction band at x = 0 to 1 are reported in this study as detailed in Table 2. Non- linear decrease in energy band gaps was observed from x =0 to 0.75 as the dopant Cr atom, which was added to replace the Sn atom, increased. Bloch vector K is taken along the high symmetry paths of Brillouin zone $\Gamma \rightarrow Z \rightarrow A \rightarrow M \rightarrow \Gamma \rightarrow X \rightarrow R \rightarrow Z$ as indicated in the figures. The direct energy gap of SnO_2 at $X \rightarrow X$ (1.16 eV) is in close agreement with Deligoz et al., (2007) at $\Gamma \rightarrow \Gamma$ (1.25 eV), even though Deligoz et al., used another high symmetry paths; $R \rightarrow \Gamma \rightarrow X \rightarrow M \rightarrow \Gamma$. An increase in band gaps at x = 1 for CrO_2 was also discovered. The calculated bowing constants as given by the semi-empirical formula in equation (2) for both direct and indirect energies are: 0.38eV and 8.28eV, respectively.

Table 2: Energy band gap of $Cr_x Sn_{1-x} O_2$ compounds in eV.

Materials	**Direct Energy**	**Band Symmetry**	**Indirect Energy**	**Band Symmetry**
SnO_2	1.16	X- X	5.56	Z - M
$Cr_{0.25}Sn_{0.75}O_2$	1.11	M - M	2.29	Z - M
$Cr_{0.50}Sn_{0.50}O_2$	0.335	X- X	1.85	Z - A
$Cr_{0.75}Sn_{0.25}O_2$	0.52	X- X	1.62	A - R
CrO_2	0.69	X- X	1.68	A - M

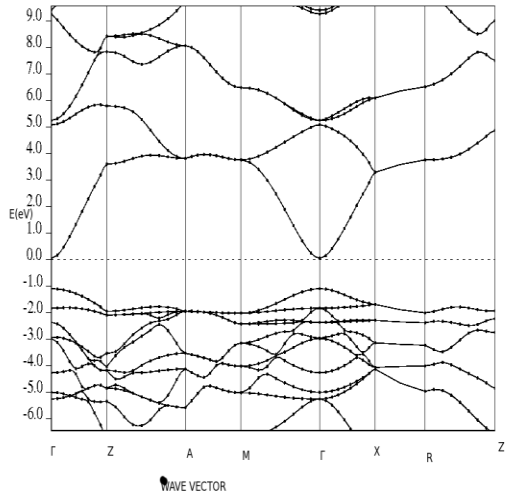

Figure 1a: Band structure of SnO_2.

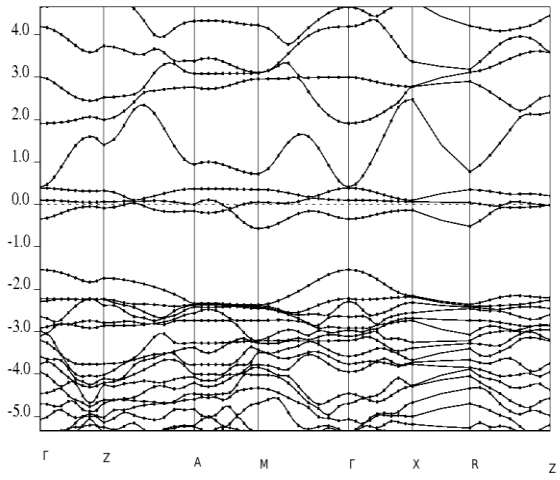

Figure 1b: Band structure of $Cr_{0.25}Sn_{0.75}O_2$

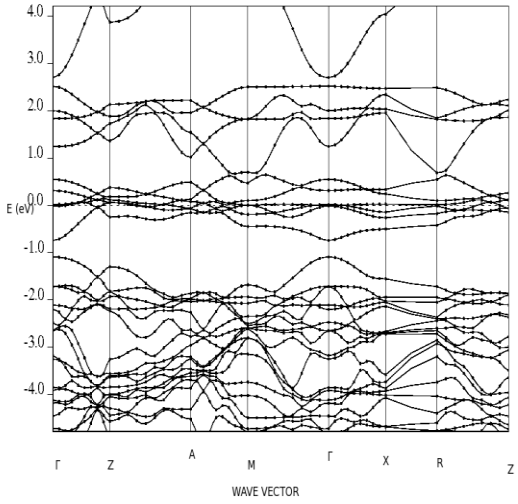

Figure 1c: Band structure of $Cr_{0.50}Sn_{0.50}O_2$.

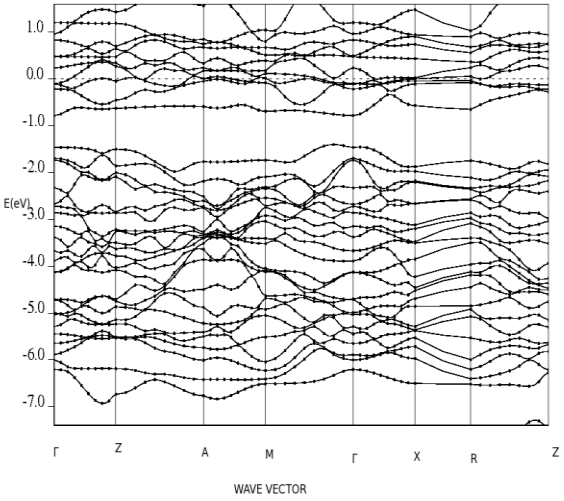

Figure 1d: Band structure of $Cr_{0.75}Sn_{0.25}O_2$.

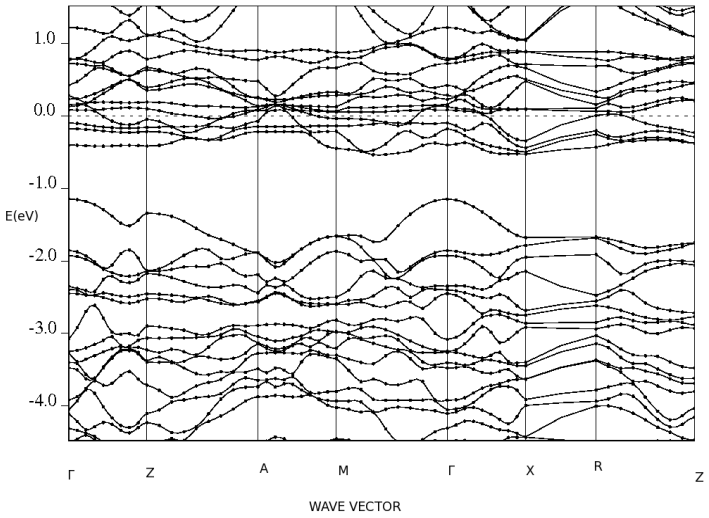

Figure 1e: Band structure of CrO_2.

Figures 2 a-d stand for density of state of $Cr_x Sn_{1-x} O_2$ compound at x = 0 to 0.75. There was no convergence at x = 1.0 due to artefacts present in the GGA approximation. The figures affirm the semiconductor properties of the materials. The uppermost valence band is principally dominated by the O- 2p state. The conduction band comprise of Sn-$5p^2$ and Cr-$3d^5$ $4S^1$ at x = 0.25 to 0.75. When x = 1.0, it is mainly dominated by Cr-$3d^5$ $4S^1$ for CrO_2**.**

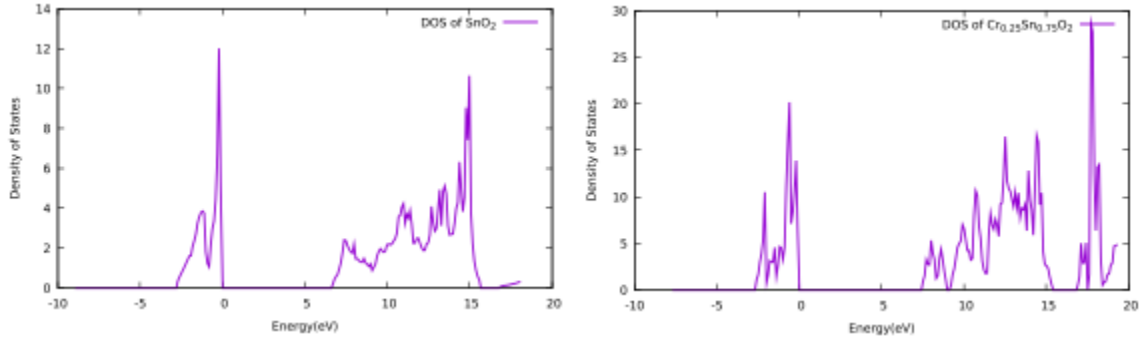

(a) Density of state of SnO_2 (b) Density of state of $Cr_{0.25}Sn_{0.75}O_2$

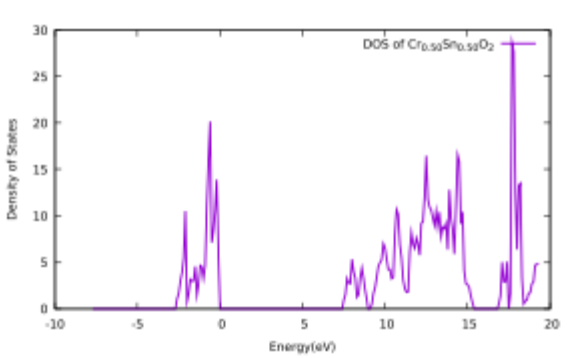

(c) Density of state of $Cr_{0.5}Sn_{0.5}O_2$

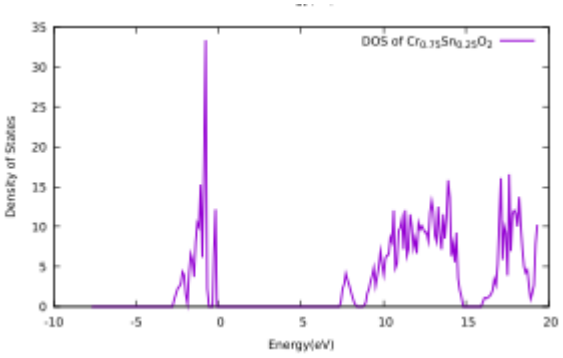

(d) Density of state of $Cr_{0.75}Sn_{0.25}O_2$

4.3 Mechanical Properties

The values of examined elastic constants of bulk, Young's, Shear, Poisson's ratio, Debye temperature and sound velocities differed with increased atoms of Cr at x = 0, 0.25, 0.50, 0.75 and 1.00. C_{11}, C_{44} and C_{66} rose with increased Cr atom from x = 0 to 1 and C_{12}, C_{13} and C_{44} increased nonlinearly with additional Cr atom substituted into the material. The values obtained at x = 0.25 to 0.75 are not yet reported in the literature. In this work, the least value of bulk modulus is observed at x = 0.5. The computed elastic constants of $Cr_x Sn_{1-x} O_2$ at x = 0, 0.25, 0.50, 0.75 and 1 are put on display in Table 3. And the variation of Young's modulus, Shear modulus, Poisson's ratio, Debye's temperature and sound velocities with concentration x is presented in Table 4.

Table 3: Elastic constant C_{ij} (GPa) and the bulk modulus B (GPa) of $Cr_x Sn_{1-x} O_2$ compound at various compositions.

Material	Techniques	C_{11}	C_{12}	C_{13}	C_{33}	C_{44}	C_{66}	B
SnO_2	Present Work(GGA)	115.9	211.5	753.4	274.3	83.7	174.3	167.1
SnO_2	Experiment	261.7	177.2	155.5	449.6	103.7	207.4	212.3
SnO_2	Others Theory(LDA)	261.3	180.3	149.9	472.1	108.5	223.7	212.6
SnO_2	Others Theory (LDA)	204.8	132.7	121.7	332.7	86.0	175.6	163.12
$Cr_{0.25}Sn_{0.75}O_2$	Present Work(GGA)	138.4	338.9	785.5	311.2	80.5	164.9	158.6
$Cr_{0.50}Sn_{0.50}O_2$	Present Work(GGA)	398.1	489.5	224.4	87.6	167.1	174.1	87.5
$Cr_{0.75}Sn_{0.25}O_2$	Present Work(GGA)	436.5	108.5	274.7	108.5	198.4	194.1	112.6
CrO_2	Present Work(GGA)	488.7	716.9	178.9	103.9	169.2	191.1	101.6
CrO_2	Others (Theory)	378	217	187	495	143	237	269

Table 4: Calculated Young's modulus (Y), Shear modulus (G), Poisson's ratio (n), Debye's temperature (Θ) and sound velocities in kms^{-1} of $Cr_xSn_{1-x}O_2$ compound at various compositions

Materials	Method	Y(GPa)	G (GPa)	n	Θ	V_p	V_B	V_G
SnO_2	Present Study	216.9	84.6	0.28	498.35	6.55	5.06	3.60
SnO_2	Previous Study	269.2	104.4	0.29	537	6.75	-	-
$Cr_{0.25}Sn_{0.75}O_2$	Present Study	224.6	88.8	0.26	537.30	6.73	5.09	3.81
$Cr_{0.50}Sn_{0.50}O_2$	Present Study	224.7	87.47	0.28	564.04	7.11	5.50	3.89
$Cr_{0.75}Sn_{0.25}O_2$	Present Study	282.9	112.63	0.26	685.97	8.04	6.04	4.60
CrO_2	Present Study	258.8	101.57	0.27	709.80	8.32	6.37	4.64
CrO_2	Previous Study	359	140	0.28	-	-	-	-

Poisson's ratio measures the ratio of lateral strain to longitudinal strain, and its maximum value for an ideal in-compressible material is 0.5. In Engineering and material sciences, it varies between 0.25 and 0.33. The values of Poisson's ratio at x = 0 to 1 in $Cr_xSn_{1-x}O_2$ compound range from 0.26 to 0.28. This made the materials with Poisson's ratio (n > 0.26) at x = 0, 0.50, 0.75 and 1.0 to be ductile and stable, as shown in Table 4, which implies high ionic bonding exists between the materials. $Cr_xSn_{1-x}O_2$ compound at various compositions with increased Debye temperature from x = 0 to 1 maintained ionic bonding in the tetragonal rutile space group $P4_2/mnm$.

5. CONCLUSIONS

In this study, analyses of structural, electronic and elastic properties of $Cr_xSn_{1-x}O_2$ compound from ab-initio calculations based on density functional theory were made. The compound minimized lattice parameters of SnO_2 are in excellent agreement with the experimental. The calculated compressive wave velocity, V_p of SnO_2 (6.55km/s) is in close agreement with value obtained from Ozer and Cabuk in 2019 (6.75 km/s) and a bit lower than that of experimental value of 7.02 km/s with a percentage error of 6.7%. From the elastic constants calculations, Debye temperature, Young's and Shear moduli as well as Poisson's ratio were assessed. Howbeit there are no experimental and theoretical values in literature to compare the structural, electronic, elastic properties with at x = 0.25 to 0.75. The experimentalists and theoreticians are employed to work on these.

REFERENCES

Al – Saadi, T. M., Hussein, B. H., Hassan, A. B., Shehab, A. A. (2019). Study the structural and optical properties of Cr doped SnO_2 nanoparticles synthesized by Sol-Gel method. *Energy Procedia volume*, 157, 457-465.

Akgul, F. A., Gumus, C., Er, A. O., Farha, A. H., Akgul, G., Ufukktepe, Y., Liu, Z. (2013). Structural and electronic properties of SnO_2. *Journal of Alloys and Compounds*, 579, https://doi.org/10.1016/j.jallcom.2013.05.057.

Arlingus, F. J. (1974). Energy Bands in Stannic Oxide. *Journal of Physics and Chemistry of Solids*, 35(8), 931-935. https://doi.org/10.1016/S00223697(74)80102-2

Bejtka, K., Zeng, J., Sacco, A., Castelline, M., Hernandez, S., Farkhondehfal, M. A., Savino, U., Ansaloni, S.; Candido, F.; Chiod, P.; Chiod, A.(2019). Chainlike Mesoporous SnO_2 as a Well- Performing Catalyst for Catalyst for Electrochemical CO_2 Reduction. *ACS Applied Energy Materials*, 2(5), 3081-3091. https://doi.org/10.1021/acsaem.8b02048

Berger, J. A., Reining, L., Sottile, F. (2010). *Physical Review B*, 82, 041103(R), DOI:10.1103/PhysRevB.82.041103

Bendaoud, H., Obodo, K.O., Bouhafs, B. (2019). *Computational Condensed Matter 21 e00400*, https://doi.org/10.1016/j.cocom.2019.e004009.

Birch, F. (1947). Finite elastic strain of cubic crystals. *Physical Review 71*, 809-824. DOI: https://doi.org/10.1103/PhysRev.71.809

Biswal, R., Nayak, D., Janakiraman, S., Chaudhary, N. V. P., Ghosh, S., Adyam, V. (2021). Revisiting and enhancing electrochemical properties of SnO_2 as anode for sodium-ion batteries. *Journal of Solid State Electrochemistry*, 25, 561- 573.

Borges, P. D., Scolfaro, L. M. Alves, H.W. L., Silva, E. F., Assali, L. V. C. (2011). Electronic and magnetic properties of SnO_2/CrO_2 thin superlattices. *Nanoscale Research Letters*, 6 (1), 146. DOI: 10.1186/1556-276X-6-146

Brener, N. E., Tyler, J. M., Callaway, J., Bagayoko, D., Zhao, G. L. (2000). *Physical Review* B, 61(24), DOI:10.1103/PhysRevB.61.16582.

Das, P. K., Chowdhury, A., Manda, N., Arya, A. (2016). *Philosophical Magazine*, 96(18), 1-22. https://doi.org/10.1080/14786435.2016.1177228

Das, S., Jayaraman, V. C. (2014). SnO_2: A comprehensive review on structures and gas sensors. *Progress in Materials Science*, 66, 112- 255. https://doi.org/10.1016/j.pmatsci.2014.06.003

Deligoz, E., Colakoglu, K., Ciftci, Y.O. (2007). The structural, elastic and electronic properties of the pyrite-type phase of SnO_2. *Journal of Physics and Chemistry of Solids*, 69(4), 859-864. https://doi.org/10.1016/j.jpcs.2007.09.019

Diliegros-Godines, C.J., Flores-Ruiz, F. J., Castanedo P. R., Torres-Delgado, G., Espinoza- Beltran, F.J., Broitman, E. (2015). Mechanical and tribological properties of CdO + SnO_2 thin films prepared by sol-gel. *Journal of Sol-Gel Science and Technology*, ISSN 0928-0707, E-ISSN 1573-4846, 74(1), 114-120.

Fakhim, L.A., Belaiche, M., Benyoussef, A., El, K. (2014). Electronic structures and ferromagnetism of SnO_2 (rutile) doped with double-impurities: First-principles calculations. *Journal of Applied Physics*, 115, 013910-0139105. https://doi.org/10.1063/1.4852475

Fitzgerald, C.B., Venkatesan, M., Dorneles, L.S., Gunning, R., Stamenov, P., Coey, J. M.D., Stampe, P. A., Kennedy, R. J., Moreira, E. C., Sias, U. S. (2006). Magnetism in dilute magnetic oxide thin films based on SnO_2. *Physical Review B*, 74(11), 115307. doi:10.1103/PhysRevB.74.115307

Gao, Q., Jiang, H., Li, M., Lu, P., Singh, M., Lai, X., Li, X., Liu, Y., Song, C. (2014). Improved mechanical properties of SnO_2: F thin film by structural modification. *Ceramics International*, 40(2), 2557-2564.

Gheonea, R., Mak, C., Crasmareanu, C. E., Simulescu, V., Plesu, N., Ilia, G. (2017). Surface Modification of SnO_2 with Phosphonic Acids. Journal of Chemistry, https://doi.org/10.1155/2017/2105938

Godinho, K.G., Walsh, A., Watson, G.W. (2009). Energetic and Electronic structure analysis of intrinsic defects in SnO_2. *Journal of Physical Chemistry C*, 113(1), 439-448. DOI:10.1021/JP807753T

Gorai, S. (2018). Bio-based Synthesis and Applications of SnO_2 Nanoparticles- An Overview. *Journal of Materials and Environmental Sciences*, 9(10), 2894- 2903.

Haeberie, J., Machulik, S., Janowitz, C., Manzke, R., Gaspa, D., Barquinha, P., SchmeiBer, D. (2016). Gap states in the electronic structure of SnO_2 single crystals and amorphous SnO_x thin films. *Journal of Applied Physics*, 120, 105101-13. https://doi.org/10.1063/1.4962313

Henkel, K., Haeberie, J., Muller, K., Janowitz, C., Schmeiber, D. (2019). Preparation, properties and electronic structure of SnO_2. Single Crystals of Electronic Materials: Growth and Properties Publisher: *Elsevier. Wood-head Publishing Series in Electronic and Optical Materials*, 547-572. DOI:10.1016/B978-0-08-102096-8.00016-1

Huang, S., Wu, X., Niu, J., Qin, S. (2018). *RSC Advances*, 43. https://doi.org/10.1039/C8RA04537B

Ji, G. F. (2011). *Comp. Mater. Sc.* 50, 1571-1577.

Jiang, J. Z., Gerward, L., Olsen, J. S. (1983). *Scr. Mater. 44*, 2001.

Jim, W.Y., Liu, X., Yiu, W. K., Leung, Y. H., Djuris, A. B., Chan, W. K., Liao, C. Shih, K., Surya, C. (2014). The effect of different dopants on SnO_2: based dye-sesitized solar cells. *Physica Status Solidi B*, 1-5. https://doi.org/10.1002/pssb.201451256

Karmaoni, M.; Jorge, A.B.; McMillan, P. F.; Labrincha, J. A.; Tobaldi, D. M. (2018). *ACS Omega*, 3(11), 16386. https://doi.org/10.1021/acsomega.8b02860

Kasar, R. R., Gosavi, S. R., Ghosh, A., Deshpande, N. G., Sharma, R. P. (2013). Influence of Cr doping on structural, morphological and optical properties of SnO_2 thin film prepared by spray pyrolysis technique. *IOSR Journal of Applied Physics*, 7, 21-26, e-ISSN: 2278- 4861. www.iosrjournals.org

Kuriganova, A.B., Han, Vlaic, C.A., Ivanov, S., Leontyeva, D. V., Bund, A., Smirnova, N.V. (2016). Electrochemical dispersion method for the synthesis of SnO_2 as anode material for lithium ion batteries. *Journal of Applied Electrochemistry*, 46, 527-538. DOI: 10.1007/s10800-016-0936.

Lee, Seul- Gi., Han, Sang-Beom., Lee, Woo-Jun., Park, Kyung-Won. (2020). Effect of Sb-Doped SnO_2 Nanostructures on Electrocatalytic Performance of a Pt Catalyst for Methanol Oxidation Reaction. *Catalysts 10*, 866.

Leng, D., Wu, L., Jiang, H., Zhao, Y., Zhang, J., Li, W., Feng L. (2012). Preparation and Properties of SnO_2 Film Deposited by Magnetron Sputtering. *International Journal of Photoenergy*, Aricle ID 235971.

https://doi.org/10.1155/2012/235971

Letifi, H., Litaiem, Y., Dridi, D., Ammar, S., Chtourou, R. (2019). Enhanced Photocatalytic Activity of Vanadium- Doped SnO_2 Nanoparticles in Rhodamie B Degradation. *Advances in Condensed Matter Physics*. https://doi.org/10.11552019/2157428

Li, Z. Q., Yin, Y. L., Liu, X. D., Li, L. Y., Liu, H. (2009). Electronic structure and optical properties of Sb-doped SnO_2. *Journal of Applied Physics*, 106, 083701. https://doi.org/10.1063/1.3245333

Liu, Chun-Me., Chen Xiang-Rong., Ji, Guang-Fu. (2011). First-principles investigations on structural, elastic and electronic properties of SnO_2 under pressure. *Computational Material Science*, 50, 1571-1577. https://doi.org/10.1016/j.commatsci.2010.12.018

Liu, D., Wang, Y., Xu, H., Zheng, H., Zhang, T., Zhang, P., Wang, F., Wu, J., Wang, Z., Chen, Z., Li, S. (2019). SnO_2-Based Perovskite Solar Cells; Configuration Design and Performance Improvement . *Solar RRL*, 3(2). https://doi.org/10.1002/solr.201800292

Mauraya, A. K., Mahana, D., Pal, P., Singh, P., Muthusamy, S. K. (2020). Effect of bulk and surface modification of SnO_2 thin films with PDO catalyst on CO gas sensing characteristics prepared by vacuum evaporation process. *Journal of Alloys and Compound*, 843, 155979.

Mishra, R. K., Kushwaha, A., Sahay, P.P. (2015). Cr-induced modifications in the structural, photoluminescence and acetone-sensing behavior of hydrothermally synthesized SnO_2 nanoparticles. *Journals of Experimental Nanoscience*, 10(13), 1041-1056. doi:10.1080/17458080.2014.952685

Molera, T., Salvado, N., Vendrell, M. (2004). Evidence of Tin Oxide Recrystalization in Opacified Lead. *Journal of the American Ceramic Society*, 82(10), 2871-2875. DOI: 10.1111/j.1151-2916.1999.tb02170.x

Monkhorst, H. J. and Pack, J. D. (1976). *Physics Rev. B*, 13, 5188.

Murnaghan, F. D. The compressibility of media under extreme pressures. *Proc Natl AcadSci USA.*, 244-247. https://doi.org/10.1073/pnas.30.9.244

Oshima, M., Yoshino, K. (2012). Structural and Electronic structure of SnO_2/ by the First- principle study. *Materials Science Forum*, 725, 265-268.DOI:10.4028/www.scientific.net/MSF.725.265

Ozer, T., Cabuk, S. (2019). Investigation of structural and mechanical properties of SnO_2. *Materials Research Express*, 6(8). https://iopscience.iop.org/article/10.1088/2053-1591/ab1fd2/meta

Rahman, G., Garcia-Suarez, V. M., Hong, S. C.; (2008). Vacancy-induced magnetism in SnO_2. A density functional study. *Physical Review B, 78*, 184404-184409. Doi:10.1103/PhysRevB.78.184404

Rashkeev, S. N. and Lambrecht, W. R. L. (2001). *Physical Review B*, 63, 165212.

Robertson, J. (1979). Electronic structure of SnO_2, GeO_2, PbO_2, TeO_2 and MgF_2. *Journal of Physics C Solid State Physics*, 12(22): 4767. DOI:10.1088/0022-3719/12/22/018

Ren, S., Ma, S., Yang, Y., Tian, D., Cai, H., Hao, C. (2017). Enhanced dyes removal properties of hollow SnO_2 Microspheres and SnO_2@C composites. *Desalination and Water Treatment*, 57, (60).

Rieu, M., Camara, M., Tournier, G., Viricelle, J. P., Pijolat, C., de Rooij, N. F., Briand, D. (2015). Inkjet Printed SnO_2 Gas Sensor on Plastic Substrate. *Elsevier BV*, 3(2). https://doi.org/10.1016/j.proeng.2015.08.569

Sabergharesou, T., Wang, T., Ju, L., Radovanovica, P.V. Electronic structure and magnetic properties of sub-3nm diameter Mn-doped SnO_2 nanocrystals and nanowires. *Applied Physics Letters*, 103, 012401. https://doi.org/10.1063/1.4813011.

Schierbaum, K. D., Weimar, U., Gopel, W., Kowalkowsk, R. (1991). Conductance, work function and catalytic activity of SnO_2- based gas sensors. *Sensors and Actuators B: Chemical*, 3(3), 205-214.

Sharma, A., Verma, K. D., Varshney, M., Singha, D., Singh, M.; Asokan, K., Kuma, R. (2010). Effect of 100MeV O7+ ion beam irradiation on structural, optical and electronic properties of SnO_2 thin films. *Radiation Effects, Defects in Solids*, 165(12). DOI:10.1080/10420150.2010.514687.

Sikalidis, C. (2011). Advances in Ceramics-Synthesis and characterization processing and specific Applications. *Published by InTechJanezaTridine*, 9, 5100 Rijeka, Croatia, ISBN 978-953-307-505-1. https://doi.org/10.1016/j.dyepig.2010.12.013

Son, Dae-Yong., Lee, Chang-Ryul., Shin, Hee-Won., Jung, H.S., Ahn, T. K., Park, Nam-Gyu (2011). Understanding the role of the dye/oxide interface via SnO_2-based MK-2 dye-sensitized solar cells . *Physical Chemistry Chemical Physics*, 17, 15193-15200. https://doi.org/10.1039/C5CP01816A.

Topuz, B. B., Bora, G.G., Colak, M. U. (2011). The effects of tin dioxide (SnO_2) on the anataserutile phase transformation of titania (TiO_2) in mica-titania pigments and their use in paint. *Dyes and Pigments*, 90(2), 123-28. https://doi.org/10.1016/j.dyepig.2010.12.013

Trojan, J., Karolova, L., Luxova, J., Trojan, M. (2016). Synthesis of SnO_2/Cr Pigments Doped by Praseodymium Prepared by Different Methods and their Pigmentary Properties. Ceramic-Silikaty 60. http://hdl.handle.net/10195/67551

Yang, H. M., Hu, Y. H. (2006). Applications of Sb-SnO_2/barite(SSB) conductive powder in conductive paint and shield property of coated layer. *Journal of Functional Materials*, 63(1), 34-39.

Yao, W., Wu, S., Zhan, L., Wang, Y. (2019). Two-dimensional porous carbon-coated sandwich- like mesoporous SnO_2/graphene/mesoporous SnO_2 nanosheets towards high-rate and long cycle life lithium-ion batteries. Chemical Engineering Journal 361, 329-341. https://doi.org/10.101016/j.cej.2018.08.217